

UC Irvine

UC Irvine Previously Published Works

Title

Hybrid diffusion and two-flux approximation for multilayered tissue light propagation modeling.

Permalink

<https://escholarship.org/uc/item/4jd27582>

Journal

Applied Optics, 50(21)

ISSN

1559-128X

Authors

Yudovsky, Dmitry

Durkin, Anthony J

Publication Date

2011-07-20

DOI

10.1364/ao.50.004237

Copyright Information

This work is made available under the terms of a Creative Commons Attribution License, available at <https://creativecommons.org/licenses/by/4.0/>

Peer reviewed

Published in final edited form as:

Appl Opt. 2011 July 20; 50(21): 4237–4245.

Hybrid diffusion and two-flux approximation for multilayered tissue light propagation modeling

Dmitry Yudovsky* and Anthony J. Durkin

Laser Microbeam and Medical Program, Beckman Laser Institute, University of California, Irvine, 1002 Health Sciences Road, Irvine, California 92612

Abstract

Accurate and rapid estimation of fluence, reflectance, and absorbance in multilayered biological media has been essential in many biophotonics applications that aim to diagnose, cure, or model *in vivo* tissue. The radiative transfer equation (RTE) rigorously models light transfer in absorbing and scattering media. However, analytical solutions to the RTE are limited even in simple homogeneous or plane media. Monte Carlo simulation has been used extensively to solve the RTE. However, Monte Carlo simulation is computationally intensive and may not be practical for applications that demand real-time results. Instead, the diffusion approximation has been shown to provide accurate estimates of light transport in strongly scattering tissue. The diffusion approximation is a greatly simplified model and produces analytical solutions for the reflectance and absorbance in tissue. However, the diffusion approximation breaks down if tissue is strongly absorbing, which is common in the visible part of the spectrum or in applications that involve darkly pigmented skin and/or high local volumes of blood such as port-wine stain therapy or reconstructive flap monitoring. In these cases, a model of light transfer that can accommodate both strongly and weakly absorbing regimes is required. Here we present a model of light transfer through layered biological media that represents skin with two strongly scattering and one strongly absorbing layer.

1. Introduction

The radiative transfer equation (RTE) is an accurate description of light propagation in biological tissue. However, exact solutions to the RTE are known only for a few idealized cases [1,2]. Monte Carlo simulations offer an accurate solution of the RTE. However, these are computationally intensive and may not be suitable for real-time applications when immediate estimation of light propagation is required. The diffusion approximation is frequently used in biomedical optics because it can be a computationally fast method for estimating light transport in strongly scattering biological tissues. Multiple adaptations of the diffusion approximation exist that account for index mismatch [3], multilayered tissue structure, and nondiffuse light sources such as collimated irradiation in plane-parallel media [4].

The simplicity and speed of the diffusion approximation when compared with Monte Carlo simulations [5] or discrete ordinates methods [1] makes it an appealing candidate for biophotonics work. However, its applicability is limited to the near infrared (NIR) since visible light is strongly absorbed by the melanin of the epidermis and the blood in the dermis [6,7]. This may not pose a significant problem for tissue spectroscopy, which takes

advantage of the deep penetration of NIR light in tissue. However, estimation of energy deposition in thin, strongly absorbing layers may be strongly affected by the assumptions implicit within the diffusion approximation. Within the context of tissue spectroscopy, these limitations are often realized as underestimated local oxyhemoglobin and deoxyhemoglobin concentrations. Specifically, for reconstructive flap monitoring and assessment of port-wine stain response to laser therapy [8–10], prediction of oxyhemoglobin and deoxyhemoglobin concentrations becomes inaccurate with increased skin pigmentation. Here we present a method for estimating the diffuse reflectance and absorbance of three layers, one-dimensional media with both strongly absorbing and scattering layers and an index mismatch at the air–tissue interface, irradiated by normal, collimated light. Additionally, radiative transfer in strongly absorbing layers was modeled with the two-flux approximation instead of the diffusion model. Unlike the diffusion approximation, the two-flux approximation is well adapted to modeling light propagation through thin, strongly absorbing layers [1].

The three layer model’s accuracy was assessed on optical properties typical of skin with three regions corresponding to the nonmelanized weakly pigmented layers of epidermis (stratum corneum, stratum lucidum, stratum granulosum, and stratum spinosum), the melanosome-rich layer of the epidermis (stratum basale), and the vascularized dermis. However, this model is broadly applicable to any three-layer medium in which the second layer is strongly absorbing. Monte Carlo simulations are used as a reference or “gold standard” for the purpose of comparison to the results obtained using the three-layer analytic model developed here.

2. Background

A. Skin Structure

The human skin consists of the epidermis and dermis. The cells in the epidermis include the basal keratinocytes, melanocytes, and Langerhans [11]. Melanocytes synthesize melanin, the skin protein mainly responsible for racial and seasonal variation of skin color. Melanin is contained in organelles known as melanosomes which are bundled in a layer close to the basement membrane [11,12]. Depending on genetic factors and UV light exposure, melanosomes occupy 1 to 43% of the epidermal volume corresponding to lightly or darkly pigmented skin, respectively [11–14]. They are found in great concentration near the basement membrane [15–17]. In normal skin, melanin absorption dominates the total absorption in the epidermis in the visible range and NIR [11–14,18]. Keratinocytes are the predominant cell type in the epidermis [11,14]. These cells form a barrier against environmental damage from bacteria, fungi, parasites, viruses, heat, UV radiation, and dehydration. Langerhans cells are dendritic, immunologically active cells derived from bone marrow that play a significant role in immune response to infection [11].

Depending on anatomic location, epidermal thickness ranges between tens to hundreds of micrometers and consists of five layers. In descending order, these layers are the stratum corneum, stratum lucidum, stratum granulosum, stratum spinosum, and stratum basale. The deepest layer, the stratum basale, consists mainly of divided and undivided keratinocytes and melanocytes. As keratinocytes reproduce and mature, they migrate toward the stratum spinosum. The stratum spinosum—also known as the “spinous” or “prickle cell” layer—consists of 8 to 10 layers of keratinocytes. The stratum granulosum is the middle layer of the epidermis. It consists of three to five layers of keratinocyte cells with lamellar and keratohyalin granules. The stratum lucidum is the second layer of the epidermis. It is most pronounced in soles of the feet and the palms of the hands where the skin is exposed to high friction. The stratum lucidum is clear and composed of three to five layers of dead keratinocyte cell layers. The most outer layer of the epidermis, the stratum corneum, is

composed of 25 to 30 layers of dead keratinocytes cells embedded in a lipid matrix. The dead cells are completely dehydrated, keratinized, and lack internal structure. They are continuously shed and replaced by cells from deeper strata, a process called desquamation.

The dermis, located beneath the epidermis, is responsible for the skin's pliability, mechanical resistance, and temperature control. The dermis is primarily composed of collagen fibers, nerves, capillaries, and blood vessels, but also contains elastin, fibroblasts, and Schwann and endothelial cells [11,12]. Collagen fibers make up 70% of the dermis, giving it strength and toughness. Elastin maintains normal elasticity and flexibility. The thickness of the dermis ranges between 450 and 650 μm [19–22]. The dermis consists of the papillary and reticular dermal layers. The papillary dermis connects the epidermis to underlying tissue and consists of long, thin, randomly oriented collagen fibers. Thicker bundles of collagen run parallel to the skin surface in the deeper reticular layer. Fibroblasts in the dermis produce collagen, elastin, and structural proteoglycans along with immunocompetent mast cells and macrophages. Depending on body location and tissue health, the volume of blood in the dermis ranges between 0.2 and 7% [14,23]. Approximately half of the blood volume is occupied by erythrocytes (red blood cells) that are responsible for oxygen transfer from the lungs throughout the body. Erythrocytes are composed mainly of hemoglobin molecules which reversibly bind to oxygen molecules in the lungs to form oxyhemoglobin. Hemoglobin is known as deoxyhemoglobin once it has released its oxygen molecules. Hemoglobin absorption dominates the total absorption in the dermis in the visible range and NIR [11,12,18].

In this study, we assume that human skin can be approximated by three layers. The first layer represents the part of the epidermis that is not pigmented by melanin and consists of the stratum corneum, stratum lucidum, stratum granulosum, and stratum spinosum. The second layer represents the part of the epidermis that contains melanosomes, the stratum basale. The third layer represents the dermis that is pigmented by blood.

B. Radiative Transfer Through Media

Propagation of electromagnetic waves in scattering media can be described with the steady state RTE [1,2]

$$\hat{s} \cdot \nabla I(\hat{r}, \hat{s}) = -(\mu_a + \mu_s)I(\hat{r}, \hat{s}) + \mu_s \int_{4\pi} I(\hat{r}, \hat{s}_i) \Phi(\hat{s}_i, \hat{s}) d\Omega_i + Q(\hat{r}, \hat{s}), \quad (1)$$

where the intensity at location \hat{r} and in direction \hat{s} is denoted by $I(\hat{r}, \hat{s})$ and expressed in $\text{W}/\text{mm}^2 \cdot \text{sr} \cdot \text{nm}$. The linear absorption and scattering coefficients are denoted by μ_a and μ_s , respectively, and expressed in inverse millimeters. The scattering phase function denoted by $\Phi(\hat{s}_i, \hat{s})$ represents the probability that radiation propagating into the elementary solid angle $d\Omega_i$ around direction \hat{s}_i will be scattered in direction \hat{s} . The first term of the right side of Eq. (1) represents attenuation of radiation due to absorption and scattering. The second term corresponds to augmentation of radiation due to scattering from all directions \hat{s}_i into direction \hat{s} . The third term $Q(\hat{r}, \hat{s})$ represents the power injected into a unit solid angle \hat{s} in a unit volume at \hat{r} . The contribution of scattering to the overall extinction is represented by the single scattering albedo denoted by ω and defined as

$$\omega = \frac{\mu_s}{\mu_a + \mu_s}. \quad (2)$$

When ω is close to 1, the intensity $I(\hat{r}, \hat{s})$ can be expressed approximately as the sum of an isotropic fluence ϕ and a directional radiative flux j as

$$\nabla I(\hat{r}, \hat{s}) = \frac{1}{4\pi} \varphi(\hat{r}) + \frac{3}{4\pi} j(\hat{r}) \cdot \hat{s}. \quad (3)$$

Substituting Eq. (3) into Eq. (1) and then multiplying by \hat{s} and taking the integral over all solid angles yields the familiar forced diffusion approximation

$$\nabla^2 \varphi(\hat{r}) - 3\mu_a(\mu_a + \mu_s(1 - g))\varphi(\hat{r}) = -3(\mu_a + \mu_s(1 - g))q(\hat{r}), \quad (4)$$

where $q(\hat{r})$ is an isotropic source term and defined as the integral of $Q(\hat{r}, \hat{s}) \cdot \hat{s}$ over all solid angles, and g is the average cosine of the scattering phase function $\Phi(\hat{s}_i, \hat{s})$. In this study, we will only consider plane-parallel, infinite media irradiated by collimated, infinite sources. In this case, Eq. (4) can be expressed more simply as a function of depth z into the medium as

$$\frac{d^2 \varphi(z)}{dz^2} - 3\mu_a \mu_{tr} \varphi(z) = -3\mu_{tr} q(z), \quad (5)$$

where μ_{tr} equals $(\mu_a + \mu'_s)$ and $\mu'_s = \mu_s(1 - g)$ is the reduced scattering coefficient. A reduced scattering albedo ω_{tr} can also be defined as

$$\omega_{tr} = \frac{\mu'_s}{\mu_a + \mu'_s}. \quad (6)$$

Finally, the relationship between the fluence and radiative flux can be expressed as

$$j = -\frac{1}{3\mu_{tr}} \frac{d\varphi}{dz}. \quad (7)$$

C. Two-Flux Approximation

The two-flux approximation is derived from the RTE under the assumptions that (i) the medium is plane parallel, (ii) light transfer is one-dimensional, and (iii) the scattering phase function is isotropic ($\Phi(\hat{s}_i, \hat{s}) = 1$). The first and second assumptions are satisfied by the scope of this study. To satisfy the third requirement, we invoke the so-called similarity relationship that states that light transport in media with optical properties (μ_a, μ_s, g) is similar to light transport in media with (μ_a, μ'_s, g') if $\mu_s(1 - g)$ is equal to $\mu'_s(1 - g')$ [24]. If $\Phi(\hat{s}_i, \hat{s})$ is isotropic, the average cosine of the scattering phase function g' is identically 0.

The reduced scattering coefficient $\mu'_s = \mu_s(1 - g)$ under isotropic scattering conditions is similar to the scattering coefficient μ_s under anisotropic scattering conditions. Then, the RTE simplifies to a set of two coupled linear ordinary differential equations in terms of the fluence φ and radiative flux j [1],

$$\frac{1}{\mu_{tr}} \frac{d\varphi(z)}{dz} = -4j(z), \quad (8)$$

$$\frac{1}{\mu_{tr}} \frac{dj(z)}{dz} = (1 - \omega_{tr})(q(z) + \varphi(z)). \quad (9)$$

3. Analysis

Figure 1 illustrates the three-layer medium considered in this study. The three-layer structure was irradiated by a uniform, collimated, normally incident beam with infinite radius. The physical distance from the surface was denoted by z and measured in millimeters. The index of refraction of air and of the medium were taken to be $n_0 = 1.00$ and $n_1 > 1.00$, respectively.

The optical and physical characteristics of the three-layer system were chosen to correspond to experimental and biopsy measurements of human skin in the visible and NIR range [12,20–22,25–29]. Layer 1 was a slab of thickness d_1 and characterized by absorption and reduced scattering coefficients $\mu_{a,1}$ and $\mu'_{s,1}$, respectively, with $\mu'_{s,1}$ much larger than $\mu_{a,1}$. This layer represented the superficial strongly scattering layers of the epidermis and was considered to be 150 μm thick. The absorption coefficient $\mu_{a,1}$ was assumed to be less than 1 mm^{-1} while the reduced scattering coefficient $\mu'_{s,1}$ was assumed to be 1 mm^{-1} , which is in the range of reduced scattering coefficients reported for the epidermis [26–29]. Layer 2 was a slab of thickness d_2 and characterized by absorption and reduced scattering coefficients $\mu_{a,2}$ and $\mu'_{s,2}$, respectively, with $\mu_{a,2}$ larger than $\mu'_{s,2}$. This region represented the pigmented melanosome layer. It was assumed to range in thickness between 10 and 150 μm . The absorption coefficient $\mu_{a,2}$ was assumed to range between 0 and 10 mm^{-1} to include and greatly exceed the range of human skin tone variability. The reduced scattering coefficient $\mu'_{s,2}$ was assumed to be less than 1 mm^{-1} . Layer 3 was a semi-infinite layer characterized by absorption and reduced scattering coefficients $\mu_{a,3}$ and $\mu'_{s,3}$, with $\mu'_{s,3}$ much larger than $\mu_{a,3}$. This layer represented the vascularized dermis. Therefore, $\mu'_{s,3}$ was assumed to range between 0 and 0.1 mm^{-1} while the reduced scattering coefficient $\mu'_{s,3}$ was assumed to equal to 2 mm^{-1} [18].

The propagation of the fluence in the stratum corneum ϕ_1 was described by the diffusion approximation as [4]

$$\frac{d^2\phi_1(z)}{dz^2} - 3\mu_{a,1}\mu_{tr,1}\phi_1(z) = -3\mu_{tr,1}q_1(z), \quad (10)$$

where the depth-dependent source term $q_1(z)$ arises from the out-scattering of the collimated beam into the diffuse flux. It was defined as

$$q_1(z) = \mu'_{s,1}q_0 e^{-\mu_{tr,1}z}, \quad (11)$$

where q_0 was the incident optical power as suggested by Ref. [4]. The relationship between the fluence ϕ_2 and radiative flux $j_2(z)$ in the stratum basale (layer 2) was modeled as in Eqs. (8) and (9) with the two-flux approximation

$$\frac{1}{\mu_{tr,2}} \frac{d\phi_2(z)}{dz} = -4j_2(z), \quad (12)$$

$$\frac{1}{\mu_{tr,2}} \frac{dj_2(z)}{dz} = (1 - \omega_{tr,2})(q_2(z) + \phi_2(z)). \quad (13)$$

The depth-dependent source term $q_2(z)$ arises from the out-scattering of the collimated beam into the diffuse flux and is defined as [4]

$$q_2(z) = \frac{\mu'_{s,2}}{\mu'_{s,1}} q_1(z_1) e^{-\mu_{tr,2}(z-z_1)}, \quad (14)$$

where z_1 is the depth of the layer 1–2 interface and $q_1(z_1)$ is defined in Eq. (11). Finally, the propagation of the fluence in the dermis (layer 3) φ_3 was described by the diffusion approximation as

$$\frac{d^2 \varphi_3(z)}{dz^2} - 3\mu_{a,3}\mu_{tr,3}\varphi_3(z) = -3\mu_{tr,3}q_3(z), \quad (15)$$

where the depth-dependent source term $q_3(z)$ is defined as [4]

$$q_3(z) = \frac{\mu'_{s,3}}{\mu'_{s,2}} q_2(z_2) e^{-\mu_{tr,3}(z-z_2)}. \quad (16)$$

The general solution of Eqs. (10)–(16) for the diffuse fluence in all three layers was found to be

$$\varphi_1(z) = e^{-z\mu_{eff,1}} \left(C_1 e^{-2z\mu_{eff,1}} + C_2 - \frac{3e^{z(\mu_{eff,1} + \mu_{tr,1})}}{\mu'_{s,1} - 2\mu_{a,1}} q_0 \right), \quad (17)$$

$$\varphi_2(z) = \frac{1}{2} e^{-2z\mu_{eff,2}} \left(C_3 \frac{2\sqrt{3}\mu_{tr,2}}{\mu_{eff,2}} \left(1 - e^{-\frac{4z\mu_{eff,2}}{\sqrt{3}}} \right) + C_4 \left(1 + e^{-\frac{4z\mu_{eff,2}}{\sqrt{3}}} \right) \right) + q_0 \mu_{a,2} \frac{4e^{\mu_{tr,2}(z_1-z) - \mu_{tr,1}z_1}}{3\mu_{a,2} + \mu'_{s,1}} \quad (18)$$

$$\varphi_3(z) = C_5 e^{-z\mu_{eff,3}} + \frac{3\mu'_{s,1}q_0}{2\mu_{a,3} - \mu'_{s,3}} e^{-\mu_{eff,3}(z-z_2) - \mu_{eff,2}(z_1-z_2) - \mu_{eff,1}z_1}, \quad (19)$$

where $\mu_{eff,n}$ is equal to $\sqrt{2\mu_{a,n}(\mu_{a,n} + \mu'_{s,n})}$. Then, the coefficients of integration C_1 , C_2 , C_3 , C_4 , and C_5 were found by enforcing continuity influence rate and diffuse photon flux at the boundaries that separate each layer, namely

$$\varphi_1(z)|_{z=z_1^-} = \varphi_2(z)|_{z=z_1^+}, \quad (20)$$

$$\varphi_2(z)|_{z=z_2^-} = \varphi_3(z)|_{z=z_2^+}, \quad (21)$$

$$j_1(z)|_{z=z_1^-} = j_2(z)|_{z=z_1^+}, \quad (22)$$

$$j_2(z)|_{z=z_2^-} = j_3(z)|_{z=z_2^+}. \quad (23)$$

The expressions for the radiative flux in layers 1 and 3 and in layer 2 were determined according to Eqs. (7) and (13), respectively. The partial-current boundary condition relates the diffuse photon flux out of the medium to the fluence rate right below the interface and was used to account for the index mismatch between the tissue and air [3,4]. This relationship can be expressed as

$$\frac{1}{4}\varphi_1(z)\Big|_{z=0^+} + \frac{1}{2}j_1(z)\Big|_{z=0^+} = \frac{1}{4}\rho_\varphi\varphi_1(z)\Big|_{z=0^+} + \frac{1}{2}\rho_j j_1(z)\Big|_{z=0^+}, \quad (24)$$

where ρ_φ and ρ_j are the reflection coefficients of the fluence and flux, respectively, due to the index mismatch at the tissue–air boundary. These reflection coefficients were calculated by integrating the Fresnel reflection coefficient for unpolarized light over all angles of incidence [3,4]. The constants C_1 , C_2 , C_3 , C_4 , and C_5 were then found by substituting Eqs. (17)–(19) into Eqs. (20)–(24) and solving the subsequent set of five linear equations.

Then, the diffuse reflectance R_d from the tissue was defined as

$$R_d = \frac{-j_1(z)\Big|_{z=0}}{q_0}. \quad (25)$$

Additionally, the total radiative energy absorbed in layers 1, 2, and 3 were found by integrating the product of the total fluence with the layer's absorption coefficients and defined as

$$A_1 = \mu_{a,1} \int_0^{z_1} (q_1(z) + \varphi_1(z)) dz, \quad (26)$$

$$A_2 = \mu_{a,2} \int_{z_1}^{z_2} (q_2(z) + \varphi_2(z)) dz, \quad (27)$$

$$A_3 = \mu_{a,3} \int_{z_2}^{\infty} (q_3(z) + \varphi_3(z)) dz. \quad (28)$$

A. Monte Carlo Simulations

A Monte Carlo simulation is a stochastic method for solving differential equations such as the RTE [1,5] and has been applied to studies of light transport in skin. Monte Carlo simulation software developed by Wang and Jacques [5] was used to provide gold-standard estimates of the diffuse reflectance R_d and layer-specific absorbance A_1 , A_2 , and A_3 of the three-layer medium for a given n_1 , d_1 , $\mu_{a,1}$, $\mu'_{s,1}$, $\mu_{a,2}$, $\mu'_{s,2}$, $\mu_{a,3}$, and $\mu'_{s,3}$. A complete and detailed description of the implementation and theoretical underpinnings of this software is given in Refs. [5,30]. The number of photon packets per simulation was adjusted until the variance associated with the estimate of the diffuse reflectance fell below 1%. Each Monte Carlo simulation was allowed to run with 1,000,000 photon packets to satisfy this criterion.

4. Results and Discussion

A. Purely Scattering and Absorbing Layers

We first consider a limiting case where the nonmelanized epidermis is purely scattering and the melanized epidermis is purely absorbing. Admittedly, this is a nonphysiologic situation, but it serves to illustrate the performance of the three-layer model under idealized conditions. Figure 2 shows the diffuse reflectance R_d of the three-layer medium and absorption A_1 , A_2 , and A_3 in each of three layers as a function of the absorption coefficient $\mu_{a,2}$ for $n_1 = 1.4$, $d_1 = 150 \mu\text{m}$, $d_2 = 50 \mu\text{m}$, $\mu_{a,1} = 0 \text{ mm}^{-1}$, $\mu_{a,3} = 0.02 \text{ mm}^{-1}$, $\mu'_{s,1} = 1 \text{ mm}^{-1}$, $\mu'_{s,2} = 0 \text{ mm}^{-1}$, $\mu_{a,3} = 2 \text{ mm}^{-1}$, and $\mu_{a,2}$ is between 0 and 10 mm^{-1} , estimated by Monte Carlo simulations and Eqs. (25)–(28). As the absorption coefficient of the melanized layer increased from 0 to 10 mm^{-1} , the absorption of radiative energy by the melanin in this layer A_2 also increases. On the other hand, A_3 decreases since less light penetrates the melanized layer and interacts with the dermis. Additionally, the diffuse reflectance from the three-layer medium R_d decreases as more radiative energy is deposited in the melanized layer. Since the stratum corneum was assumed to be nonabsorbing, A_1 is identically 0%. Figure 2 also presents the percent relative error between the Monte Carlo simulation and the three-layer model. The relative percent error does not exceed 10% for $\mu_{a,2}$ between 0 and 10 mm^{-1} .

Figure 3 depicts estimates of the diffuse reflectance of the three-layer medium R_d and absorption in each of three layers A_1 , A_2 , and A_3 as a function of the thickness of the melanized layer d_2 between 10 and $150 \mu\text{m}$ for $n_1 = 1.4$, $d_1 = 150 \mu\text{m}$, $\mu_{a,1} = 0 \text{ mm}^{-1}$, $\mu_{a,2} = 1 \text{ mm}^{-1}$, $\mu_{a,3} = 0.02 \text{ mm}^{-1}$, $\mu'_{s,1} = 1 \text{ mm}^{-1}$, $\mu'_{s,2} = 0 \text{ mm}^{-1}$, and $\mu'_{s,3} = 2 \text{ mm}^{-1}$, estimated by Monte Carlo simulations and the three-layer analytic model. As the melanized layer thickens, the total radiative energy absorbed by melanin also increases. The melanized layer shields the dermis and so the amount of radiative energy absorbed by the dermis decreases. Additionally, the diffuse reflectance from the three-layer medium R_d decreases as more radiative energy is deposited in the melanized layer. Figure 3 also shows the percent relative error between the Monte Carlo simulation and the three-layer model. The relative percent error does not exceed 10% for d_2 between 10 and $150 \mu\text{m}$.

Figure 4 presents estimates of the diffuse reflectance of the three-layer medium R_d and absorption in each of three layers A_1 , A_2 , and A_3 as a function of the absorption coefficient $\mu_{a,3}$ for $n_1 = 1.4$, $d_1 = 150 \mu\text{m}$, $d_2 = 50 \mu\text{m}$, $\mu_{a,1} = 0 \text{ mm}^{-1}$, $\mu_{a,2} = 1 \text{ mm}^{-1}$, $\mu'_{s,1} = 1 \text{ mm}^{-1}$, $\mu'_{s,2} = 0 \text{ mm}^{-1}$, $\mu'_{s,3} = 2 \text{ mm}^{-1}$, and $\mu_{a,3}$ is between 0.001 and 0.1 mm^{-1} , estimated by Monte Carlo simulations and the three-layer analytic model. The absorption coefficient of the dermis is primarily determined by its blood content and oxygen saturation. The range of absorption coefficient was chosen to represent the human dermis with a 6.5% blood volume fraction and for oxygen saturation between 0 and 100% for the NIR range of the spectrum between 600 and 1000 nm [31]. As expected, the total absorption of the dermis A_3 increased with the increasing absorption coefficient while the absorption of light in the melanized layer and the total tissue reflectance decreased. Figure 4 also illustrates the percent relative error between the Monte Carlo simulation and the three-layer analytic model. The relative percent error does not exceed 10% for $\mu_{a,3}$ between 0.001 and 0.1 mm^{-1} . This was expected since the diffusion approximation is accurate in modeling light transfer through strongly scattering media and the single scattering albedo of the dermis for $\mu_{a,3}$ between 0.001 and 0.1 mm^{-1} and $\mu'_{s,3} = 2 \text{ mm}^{-1}$ does not fall below 0.95.

B. General Skin Model

In the previous sections, the absorption coefficient of the nonmelanized layer $\mu_{a,1}$ and the reduced scattering coefficient of the melanized layer $\mu'_{s,2}$ were considered to be identically zero. In reality, some disease formations may cause the stratum corneum, stratum lucidum, stratum granulosum, or stratum spinosum to exhibit nonzero absorption. Additionally, it is likely that the stratum basale will exhibit nonzero scattering [32]. Figure 5 reports estimates of the diffuse reflectance of the three-layer medium R_d and absorption in each of three layers A_1 , A_2 , and A_3 as a function of the absorption and scattering coefficients $\mu_{a,1}$ and $\mu'_{s,2}$, respectively, for $n_1 = 1.4$, $d_1 = 150 \mu\text{m}$, $d_2 = 50 \mu\text{m}$, $\mu_{a,2} = 0.5 \text{ mm}^{-1}$, $\mu_{a,3} = 0.01 \text{ mm}^{-1}$, $\mu'_{s,1} = 1 \text{ mm}^{-1}$, $\mu'_{s,3} = 2 \text{ mm}^{-1}$, and $\mu_{a,1} = \mu'_{s,2}$ is between 0 and 1 mm^{-1} . Figure 5 is not meant to imply that $\mu_{a,1}$ and $\mu'_{s,2}$ are or should be equal. Instead, it shows the accuracy of the three-layer analytic model when both $\mu_{a,1}$ and $\mu'_{s,2}$ depart from the range ideal for the diffusion approximation and the two-flux approximations, respectively. Despite the addition of absorption and scattering in the nonmelanized and melanized layers, respectively, the three-layer analytic model estimated the diffuse reflectance R_d and absorption A_1 , A_2 , and A_3 to within 10% of the estimate produced by Monte Carlo simulations for the range of $\mu_{a,1}$ and $\mu'_{s,2}$ reported. Note that for $\mu_{a,1}$ equaling to 1 mm^{-1} , the transport single scattering albedo of the stratum corneum and stratum basale are $\omega_{\text{tr},1} = 0.5$ and $\omega_{\text{tr},2} = 0.67$, respectively. Both layers are in a transitional regime that is neither scattering nor absorption dominated. Nonetheless, the three-layer model accurately predicts the vital reflectance and dosimetry parameters.

The layer-specific absorptions A_1 , A_2 , and A_3 are bulk quantities that can be used to estimate the amount of radiative energy deposited in a layer by the incident beam. However, estimation of the local fluence $\varphi(z)$ is required to determine parameters such as the penetration depth of light in a multi-layered medium. Figure 6 illustrated the fluence $\varphi(z)$ estimated by Monte Carlo simulations, a three-layer diffusion approximation, and the three-layer analytic model presented in this study for $n_1 = 1.4$, $d_1 = 150 \mu\text{m}$, $d_2 = 50 \mu\text{m}$, $\mu_{a,2} = 0.5 \text{ mm}^{-1}$, $\mu_{a,3} = 0.01 \text{ mm}^{-1}$, $\mu'_{s,1} = 1 \text{ mm}^{-1}$, $\mu'_{s,3} = 2 \text{ mm}^{-1}$, and $\mu_{a,1} = \mu'_{s,2} = 0.121 \text{ mm}^{-1}$. The fluence $\varphi(z)$ was evaluated as

$$\varphi(z) = \begin{cases} \varphi_1(z) & \text{for } z < z_1 \\ \varphi_2(z) & \text{for } z_1 \leq z < z_2 \\ \varphi_3(z) & \text{for } z \geq z_2 \end{cases} . \quad (29)$$

Estimates of the fluence by the three-layer analytic model and Monte Carlo simulations exhibit the characteristic subsurface maximum near the tissue surface due to the total internal reflection caused by index mismatch. This phenomenon is captured by both models; however, the subsurface maximum estimated by the Monte Carlo simulation is more pronounced than the estimate by the present model. The absolute relative difference between Monte Carlo simulations and the present hybrid model does not exceed 5.5% when z is less than 3 mm. The fluence vanishes beyond 3 mm. On the other hand, the diffusion approximation exhibits a 14% maximum absolute error when z equals 0.44 mm and is typically 10% when z is greater than 1 mm. Figure 6 illustrates that the present hybrid model greatly improves the accuracy in predicting the fluence in three-layer media over the standard diffusion approximation.

C. Effects of Refraction Index

Figure 7 reports estimates of the diffuse reflectance of the three-layer medium R_d and absorption in each of three layers A_1 , A_2 , and A_3 as a function of tissue refractive index n_1 for $d_1 = 150 \mu\text{m}$, $d_2 = 50 \mu\text{m}$, $\mu_{a,1} = 0.05 \text{ mm}^{-1}$, $\mu_{a,2} = 1 \text{ mm}^{-1}$, $\mu_{a,3} = 0.01 \text{ mm}^{-1}$, $\mu'_{s,1} = 1 \text{ mm}^{-1}$, $\mu'_{s,2} = 0.5 \text{ mm}^{-1}$, $\mu'_{s,3} = 2 \text{ mm}^{-1}$, and n_1 is between 1 and 2, estimated by Monte Carlo simulations and the three-layer analytic model. As the tissue's refractive index increases, more light is totally internally reflected at the tissue-air interface. Thus, the total diffuse reflectance R_d of the tissue decreases approximately linearly with an increasing refraction index. At the same time, the amount of radiative energy absorbed by each layer increases. Figure 7 also shows the percent relative error between the Monte Carlo simulation and the three-layer analytic model. The relative percent error does not exceed 10% for estimates of R_d , A_2 , and A_3 when n_1 is between 1 and 2. The relative percent error between Monte Carlo simulations and the present approximate model in estimating A_1 does not exceed 12% for all n_1 considered even though the total radiative energy absorbed by this layer is less than 5%.

D. Application and Limitations

Light transfer models can be useful for tissue spectroscopy and dosimetry. In the former case, the light transfer model is used to estimate tissue optical properties from a measured reflectance spectrum. In the latter case, the amount of radiative energy deposited in the tissue with known or assumed optical properties is estimated using the light transfer model. In the realm of reflectance spectroscopy, a 10% error in the forward light model may result in a large error in estimation of the absolute value of tissue optical properties. However, relative changes in optical properties can be detected readily and quantitatively with approximate models [33,34]. Furthermore, by normalizing measured reflectance to a tissue-simulating phantom with known properties, absolute estimation of tissue optical properties can be determined in a linear region close to the properties of the phantom [31]. In the realm of dosimetry, a 10% error in estimating tissue absorbance may result, for example, in a 10% underestimate of the heating rate in a tissue due to laser irradiation. However, the severity of this estimation error is application-specific and cannot be assessed in the present study.

5. Conclusion

This study proposes a model of light transfer through layered biological media with two strongly scattering and one strongly absorbing layer. The scattering layers represent the nonmelanized epidermis and dermis of skin while the absorbing layer represents a thin and strongly melanized layer between the epidermis and dermis. Light transfer through the strongly scattering and strongly absorbing layers was modeled with the diffusion and two-flux approximation, respectively. Continuity of fluence and flux was ensured at the layer boundaries and the partial-current boundary condition was used at the tissue-air interface to model the effects of index mismatch between the tissue and the air. The accuracy of the three-layer analytic model was assessed for a wide range of optical properties of human skin in the NIR. This model may be useful for estimating the reflectance and absorbance of multilayered turbid media with strongly absorbing layers. This may occur, for example, in imaging applications such as reconstructive flap monitoring when blood-engorged tissue of venous outflow is occluded or the assessment of port-wine stain response to laser therapy [8–10].

Future work will entail extending this present model to modeling the effect of spatially modulating the incident beam in an effort to adapt it to spatial frequency domain imaging techniques under development in our laboratory [31].

Acknowledgments

The authors gratefully acknowledge funding provided by the National Institutes of Health Small Business Innovation Research (NIH SBIR) 1R43RR030696-01A1, the National Institutes of Health National Center for Research Resources (NIH NCRR) Biomedical Technology Research Center (Laser Microbeam and Medical Program (LAMMP): 5P-41RR01192), the Military Photomedicine Program, Air Force Office of Scientific Research (AFOSR) grant FA9550-08-1-0538, and the Beckman Foundation.

References

1. Modest, MF. Radiative Heat Transfer. Academic; 2003.
2. Chandrasekhar, S. Radiative Transfer. Dover; 1960.
3. Haskell RC, Svaasand LO, Tsay T-T, Feng T-C, McAdams MS, Tromberg BJ. Boundary conditions for the diffusion equation in radiative transfer. *J. Opt. Soc. Am. A.* 1994; 11:2727–2741.
4. Svaasand LO, Spott T, Fishkin JB, Pham T, Tromberg BJ, Berns MW. Reflectance measurements of layered media with diffuse photon-density waves: a potential tool for evaluating deep burns and subcutaneous lesions. *Phys. Med. Biol.* 1999; 44:801–813. [PubMed: 10211811]
5. Wang L, Jacques SL, Zheng L. MCML–Monte Carlo modeling of light transport in multi-layered tissues. *Comput. Methods Programs Biomed.* 1995; 47:131–146. [PubMed: 7587160]
6. Yoon G, Prah SA, Welch AJ. Accuracies of the diffusion approximation and its similarity relations for laser irradiated biological media. *Appl. Opt.* 1989; 28:2250–2255. [PubMed: 2055507]
7. Alexandrakis G, Farrell TJ, Patterson MS. Accuracy of the diffusion approximation in determining the optical properties of a two-layer turbid medium. *Appl. Opt.* 1998; 37:7401–7409. [PubMed: 18301574]
8. Pharaon MR, Scholz T, Bogdanoff S, Cuccia D, Durkin AJ, Hoyt DB, Evans GRD. Early detection of complete vascular occlusion in a pedicle flap model using quantitation spectral imaging. *Plast. Reconstr. Surg.* 2010; 126:1924–1935. [PubMed: 21124132]
9. Jung B, Choi B, Durkin AJ, Kelly KM, Nelson JS. Characterization of port wine stain skin erythema and melanin content using cross polarized diffuse reflectance imaging. *Lasers Surg. Med.* 2004; 34:174–181. [PubMed: 15004831]
10. Yafi A, Vetter TS, Scholz T, Patel S, Saager RB, Cuccia DJ, Evans GR, Durkin AJ. Postoperative quantitative assessment of reconstructive tissue status in a cutaneous flap model using spatial frequency domain imaging. *Plast. Reconstr. Surg.* 2011; 127:117–130. [PubMed: 21200206]
11. Young AR. Chromophores in human skin. *Phys. Med. Biol.* 1997; 42:789–802. [PubMed: 9172259]
12. Anderson RR, Parrish JA. The optics of human skin. *J. Invest. Dermatol.* 1981; 77:13–19. [PubMed: 7252245]
13. Dwyer T, Prota G, Blizzard L, Ashbolt R, Vincensi MR. Melanin density and melanin type predict melanocytic naevi in 19–20 year olds of northern European ancestry. *Melanoma Res.* 2000; 10:387–394. [PubMed: 10985674]
14. Jacques, SL. Origins of tissue optical properties in the UVA, visible, and NIR regions. In: Alfano, RR.; Fujimoto, JG., editors. *OSA TOPS on Advances in Optical Imaging and Photon Migration.* Vol. 2. Optical Society of America; 1996. p. 364-369.
15. Matts PJ, Dykes PJ, Marks R. The distribution of melanin in skin determined in vivo. *Br. J. Dermatol.* 2007; 156:620–628. [PubMed: 17493065]
16. Nielsen KP, Zhao L, Stamnes JJ, Stamnes K, Moan J. The importance of the depth distribution of melanin in skin for DNA protection and other photobiological processes. *J. Photochem. Photobiol., B.* 2006; 82:194–198. [PubMed: 16388960]
17. Tadokoro T, Kobayashi N, Zmudzka BZ, Ito S, Wakamatsu K, Yamaguchi Y, Korossy KS, Miller SA, Beer JZ, Hearing VJ. UV-induced DNA damage and melanin content in human skin differing in racial/ethnic origin. *FASEB J.* 2003; 17:1177–1179. [PubMed: 12692083]
18. Saager RB, Cuccia DJ, Durkin AJ. Determination of optical properties of turbid media spanning visible and near-infrared regimes via spatially modulated quantitative spectroscopy. *J. Biomed. Opt.* 2010; 15 017012.

19. Southwood WFW. The thickness of the skin. *Plast. Reconstr. Surg.* 1955; 15:423–429.
20. Lee Y, Hwang K. Skin thickness of Korean adults. *Surg. Radiol. Anat.* 2002; 24:183–189. [PubMed: 12375070]
21. Gambichler T, Matip R, Moussa G, Altmeyer P, Hoffmann K. In vivo data of epidermal thickness evaluated by optical coherence tomography: effects of age, gender, skin type, and anatomic site. *J. Dermatol. Sci.* 2006; 44:145–152. [PubMed: 17071059]
22. Sandby-Moller J, Poulsen T, Wulf HC. Epidermal thickness at different body sites: relationship to age, gender, pigmentation, blood content, skin type and smoking habits. *Acta Derm.-Venereol.* 2003; 83:410–413. [PubMed: 14690333]
23. Krishnaswamy A, Baranoski GVG. A biophysically based spectral model of light interaction with human skin. *Comput. Graph. Forum.* 2004; 23:331–340.
24. Reindert G, Jan GA, Frits FMdM, Henk WJ. Similarity relations for anisotropic scattering in absorbing media. *Opt. Eng.* 1993; 32:244–252.
25. Tuchin, VV. *Tissue Optics.* SPIE; 2000.
26. Salomatina E, Jiang B, Novak J, Yaroslavsky AN. Optical properties of normal and cancerous human skin in the visible and near-infrared spectral range. *J. Biomed. Opt.* 2006; 11 064026.
27. Simpson CR, Kohl M, Essenpreis M, Cope M. Near-infrared optical properties of ex vivo human skin and subcutaneous tissues measured using the Monte Carlo inversion technique. *Phys. Med. Biol.* 1998; 43:2465–2478. [PubMed: 9755939]
28. Marchesini R, Clemente C, Pignoli E, Brambilla M. Optical properties of in vitro epidermis and their possible relationship with optical properties of in vivo skin. *J. Photochem. Photobiol., B.* 1992; 16:127–140. [PubMed: 1474422]
29. Wan S, Anderson R, Parrish JA. Analytical modeling for the optical properties of the skin with in vitro and in vivo applications. *Photochem. Photobiol.* 1981; 34:493–499. [PubMed: 7312955]
30. Wang L, Jacques SL, Zheng L. CONV—convolution for responses to a finite diameter photon beam incident on multilayered tissues. *Comput. Methods Programs Biomed.* 1997; 54:141–150. [PubMed: 9421660]
31. Cuccia DJ, Bevilacqua F, Durkin AJ, Ayers FR, Tromberg BJ. Quantitation and mapping of tissue optical properties using modulated imaging. *J. Biomed. Opt.* 2009; 14 024012.
32. Magnain C, Elias M, Frigerio J. Skin color modeling using the radiative transfer equation solved by the auxiliary function method. *J. Opt. Soc. Am. A.* 2007; 24:2196–2205.
33. Sassaroli A, Fantini S. Comment on the modified Beer–Lambert law for scattering media. *Phys. Med. Biol.* 2004; 49:N255. [PubMed: 15357206]
34. Kocsis L, Herman P, Eke A. The modified Beer–Lambert law revisited. *Phys. Med. Biol.* 2006; 51:N91. [PubMed: 16481677]

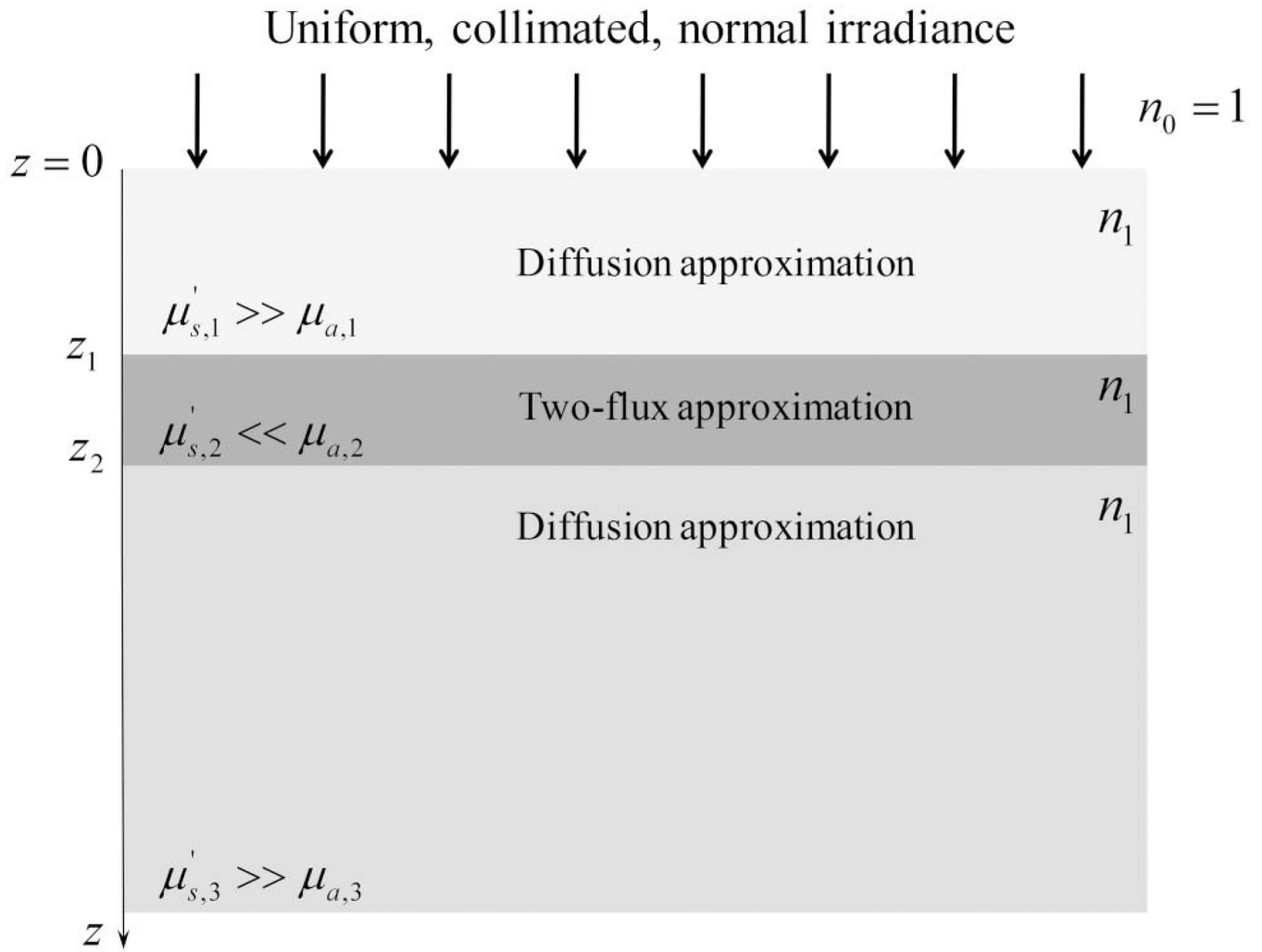


Fig. 1.
Schematic of the three-layer geometry considered.

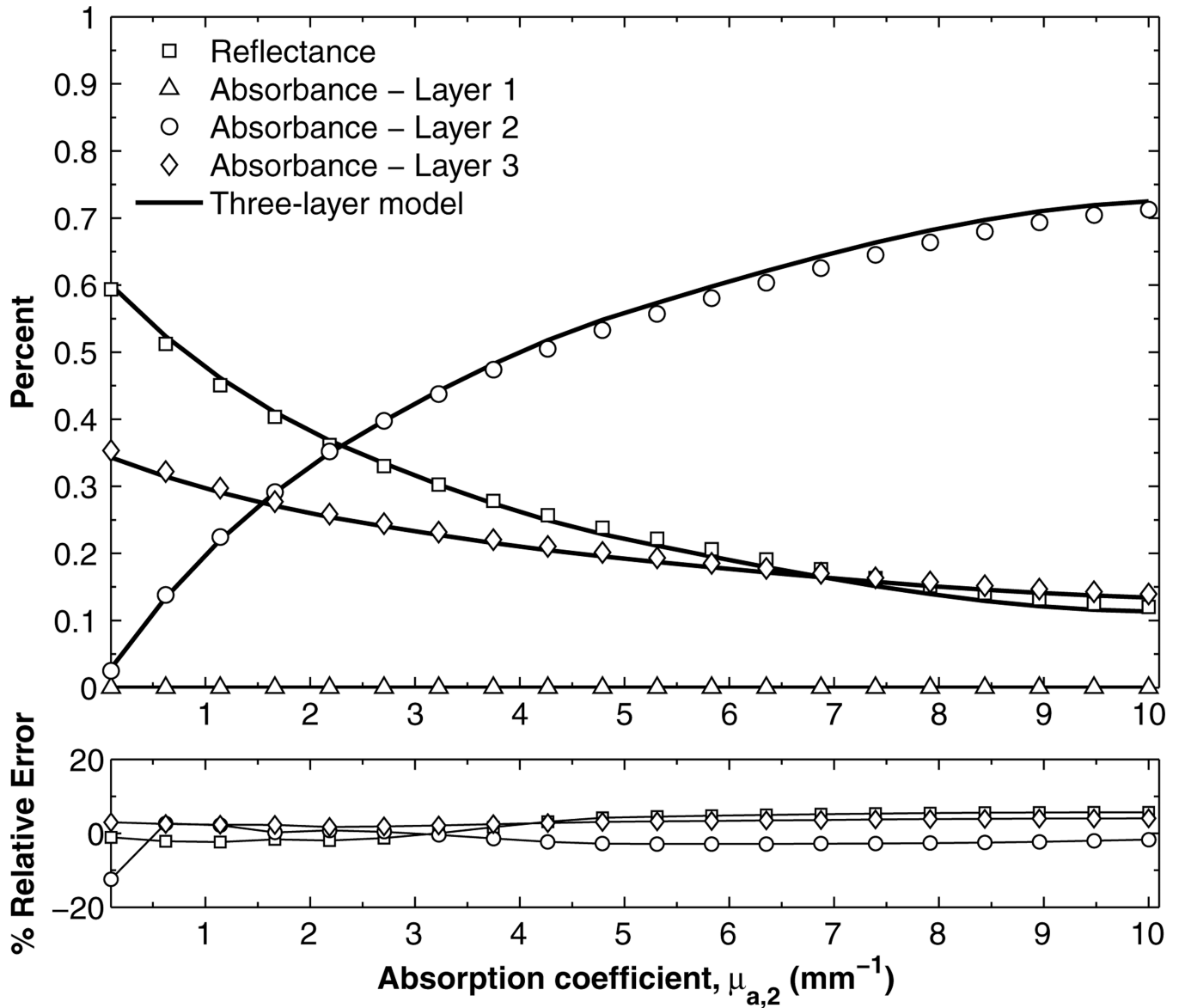


Fig. 2. Estimates of the diffuse reflectance of the three-layer medium R_d and absorption in each of three layers A_1 , A_2 , and A_3 as a function of the absorption coefficient $\mu_{a,2}$ for $n_1 = 1.4$, $d_1 = 150 \mu\text{m}$, $d_2 = 50 \mu\text{m}$, $\mu_{a,1} = 0 \text{ mm}^{-1}$, $\mu_{a,3} = 0.02 \text{ mm}^{-1}$, $\mu'_{s,1} = 1 \text{ mm}^{-1}$, $\mu'_{s,2} = 0 \text{ mm}^{-1}$, $\mu_{a,3} = 2 \text{ mm}^{-1}$, and $\mu_{a,2}$ is between 0 and 10 mm^{-1} , estimated by Monte Carlo (symbols) simulations and the three-layer analytic model (solid line). The relative percent error for each estimate is also shown.

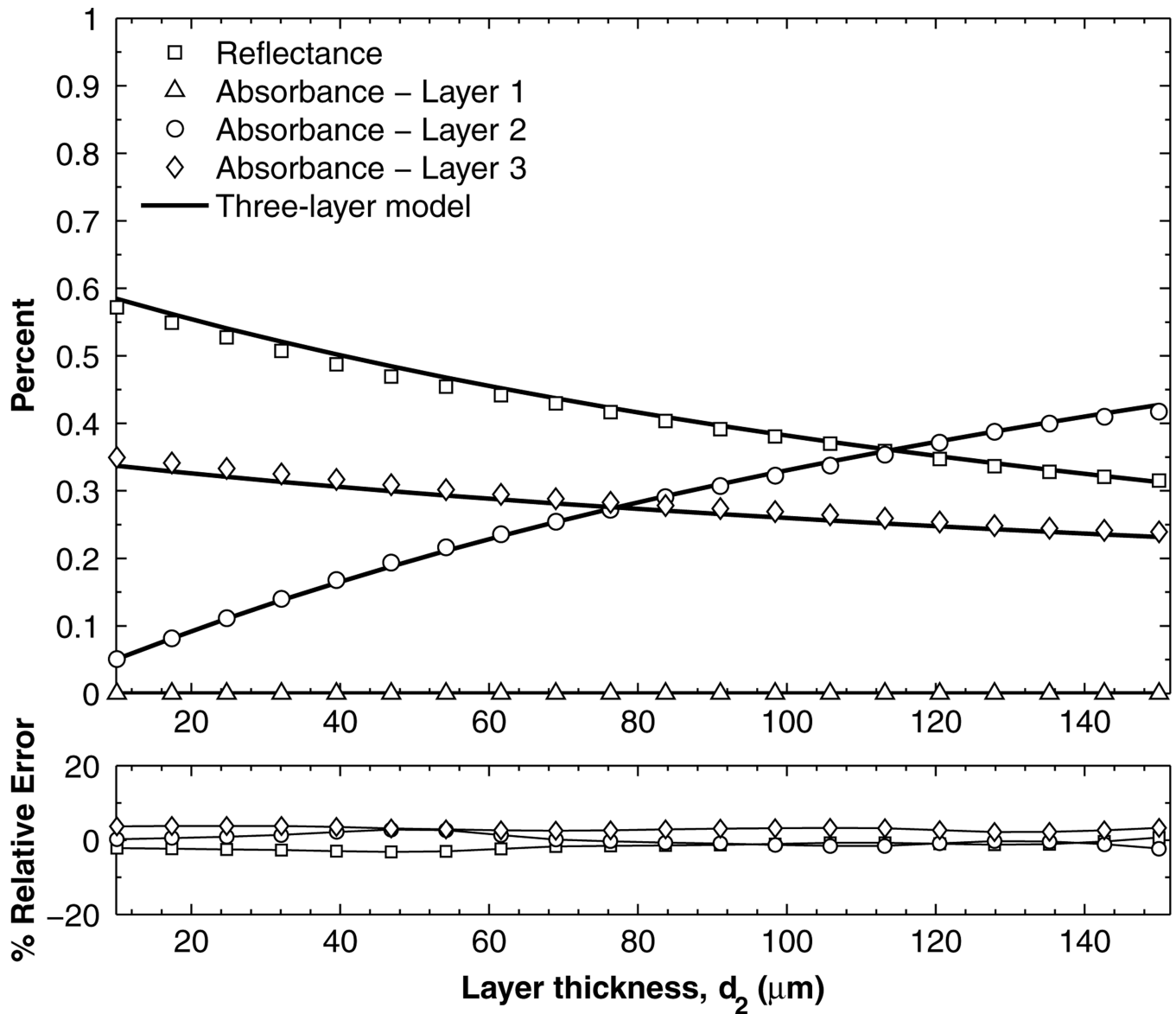


Fig. 3. Estimates of the diffuse reflectance of the three-layer medium R_d and absorption in each of three layers A_1 , A_2 , and A_3 as a function of the layer thickness d_2 for $n_1 = 1.4$, $d_1 = 150 \mu\text{m}$, $\mu_{a,1} = 0 \text{ mm}^{-1}$, $\mu_{a,2} = 1 \text{ mm}^{-1}$, $\mu_{a,3} = 0.02 \text{ mm}^{-1}$, $\mu'_{s,1} = 1 \text{ mm}^{-1}$, $\mu'_{s,2} = 0 \text{ mm}^{-1}$, $\mu'_{s,3} = 2 \text{ mm}^{-1}$, and d_2 is between 10 and 150 μm , estimated by Monte Carlo simulations (symbols) and the three-layer analytic model (solid line). The relative percent error for each estimate is also shown.

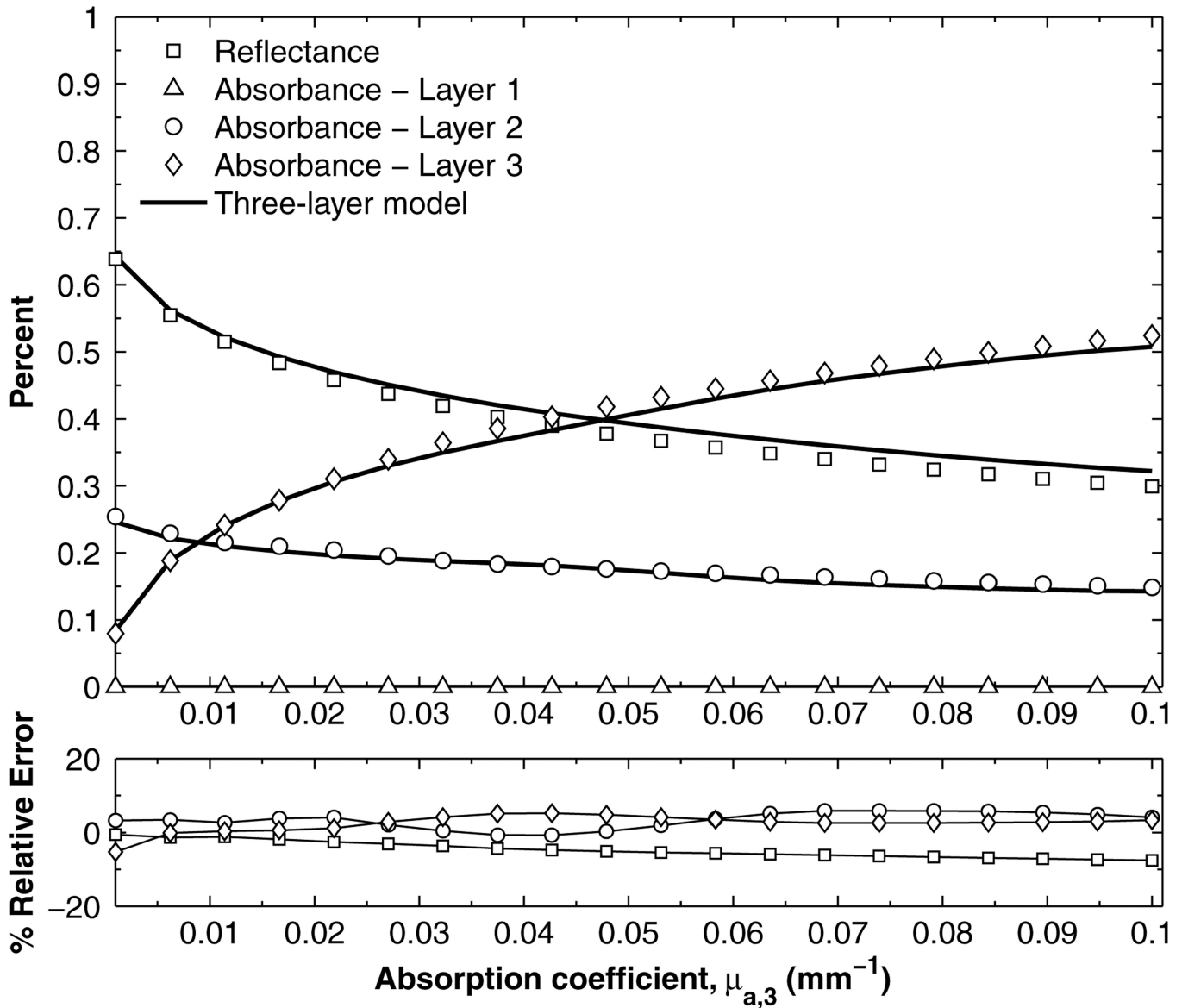


Fig. 4. Estimates of the diffuse reflectance of the three-layer medium R_d and absorption in each of three layers A_1 , A_2 , and A_3 as a function of the absorption coefficient $\mu_{a,3}$ for $n_1 = 1.4$, $d_2 = 150 \mu\text{m}$, $d_2 = 50 \mu\text{m}$, $\mu_{a,1} = 0 \text{ mm}^{-1}$, $\mu_{a,2} = 1 \text{ mm}^{-1}$, $\mu'_{s,1} = 1 \text{ mm}^{-1}$, $\mu'_{s,2} = 0 \text{ mm}^{-1}$, $\mu'_{s,3} = 2 \text{ mm}^{-1}$, and $\mu_{a,3}$ is between 0.001 and 0.1 mm^{-1} , estimated by Monte Carlo simulations (symbols) and the three-layer analytic model (solid line). The relative percent error for each estimate is also shown.

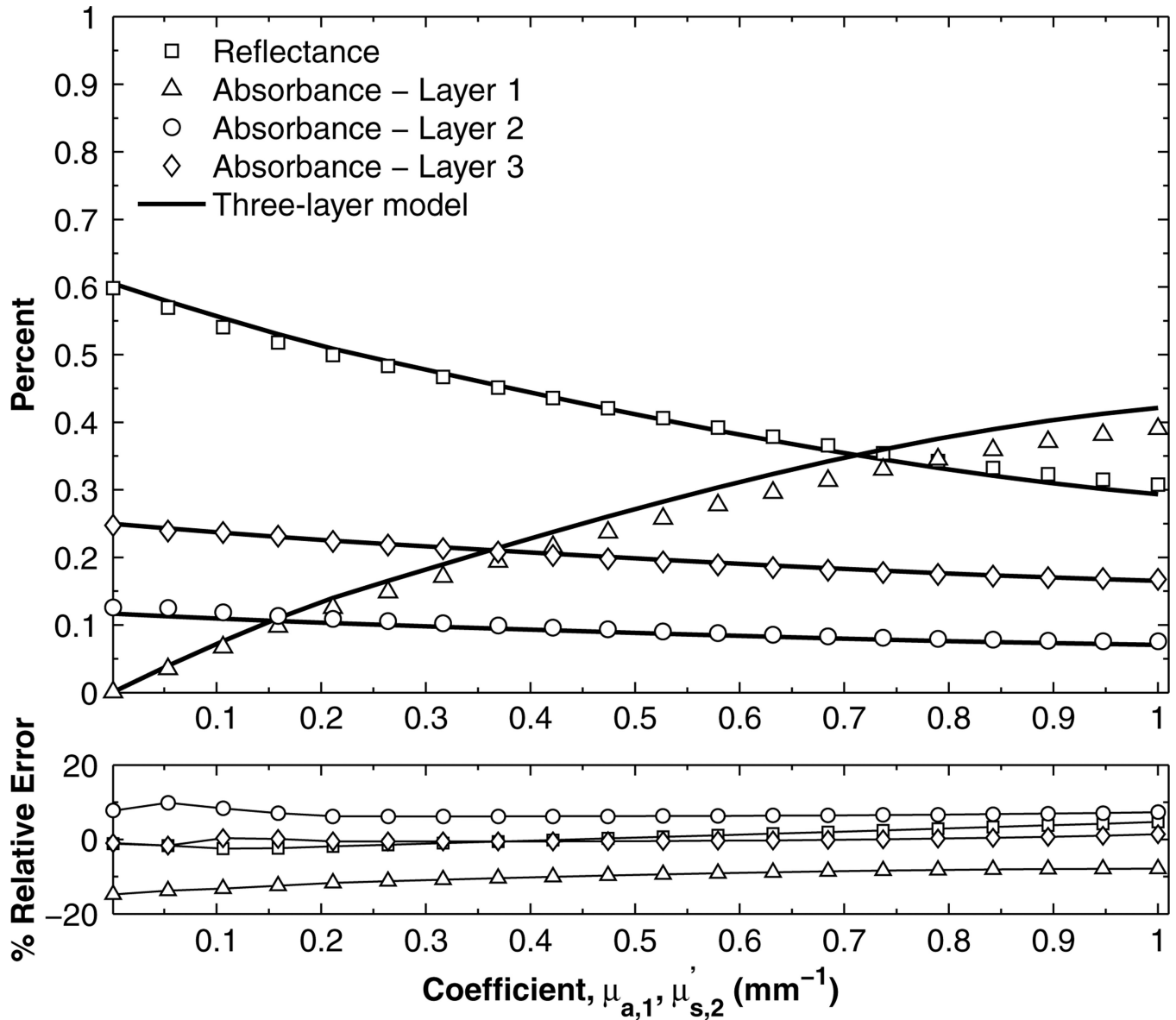


Fig. 5. Estimates of the diffuse reflectance of the three-layer medium R_d and absorption in each of three layers $A_1, A_2,$ and A_3 as a function of the absorption and scattering coefficients $\mu_{a,1}=\mu'_{s,2}$ for $n_1 = 1.4, d_1 = 150 \mu\text{m}, d_2 = 50 \mu\text{m}, \mu_{a,2} = 0.5 \text{ mm}^{-1}, \mu_{a,3} = 0.01 \text{ mm}^{-1}, \mu'_{s,1} = 1 \text{ mm}^{-1}, \mu'_{s,3} = 2 \text{ mm}^{-1},$ and $\mu_{a,1}=\mu'_{s,2}$ is between 0 and 1 mm^{-1} , estimated by Monte Carlo simulations (symbols) and the three-layer analytic model (solid line). The relative percent error for each estimate is also shown.

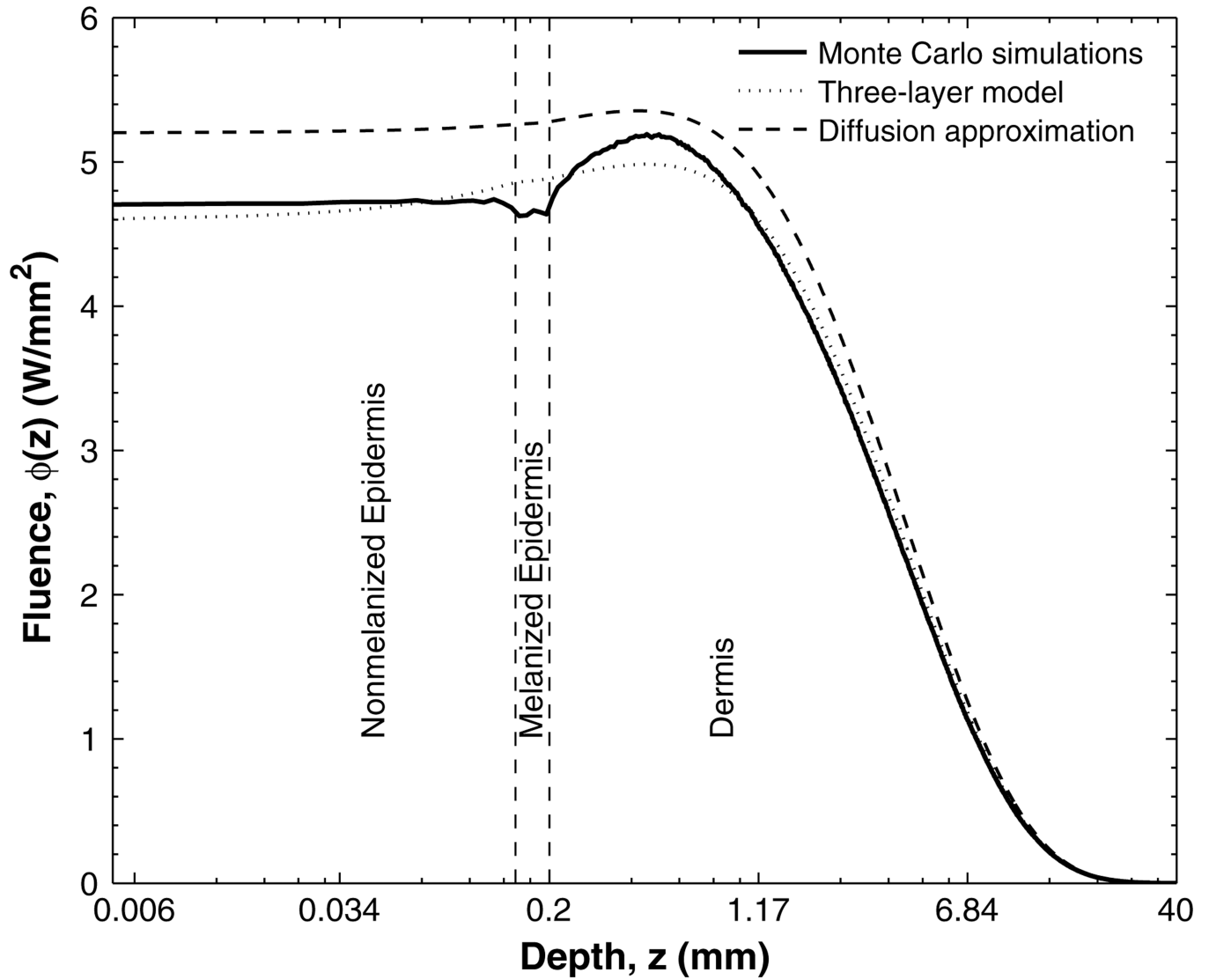


Fig. 6. The fluence $\phi(z)$ estimated by Monte Carlo simulations and the three-layer analytic model for $n_1 = 1.4$, $d_1 = 150 \mu\text{m}$, $d_2 = 50 \mu\text{m}$, $\mu_{a,2} = 0.5 \text{ mm}^{-1}$, $\mu_{a,3} = 0.01 \text{ mm}^{-1}$, $\mu'_{s,1} = 1 \text{ mm}^{-1}$, $\mu'_{s,3} = 2 \text{ mm}^{-1}$, and $\mu_{a,1} = \mu'_{s,2} = 0.121 \text{ mm}^{-1}$.

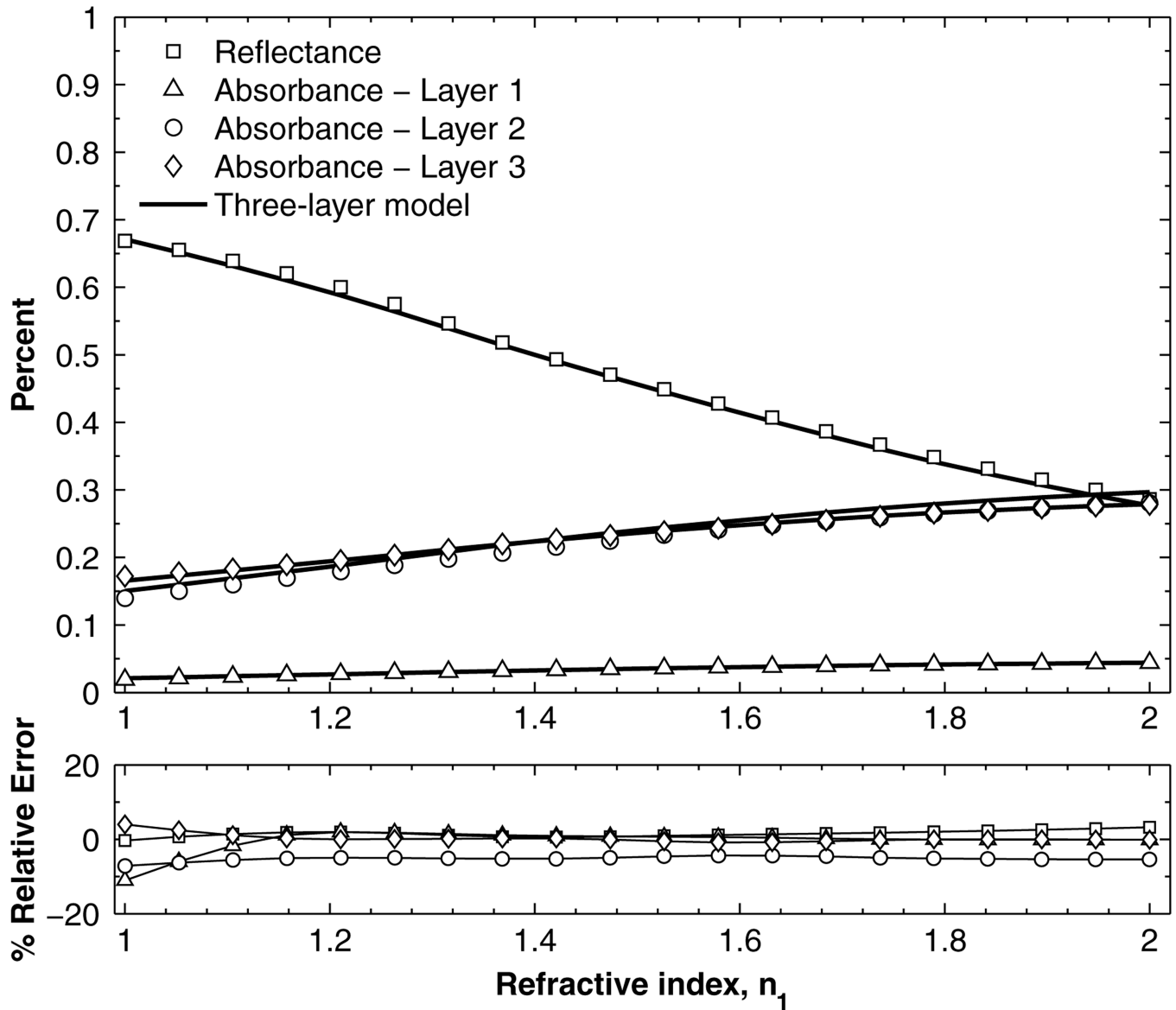


Fig. 7.

Estimates of the diffuse reflectance of the three-layer medium R_d and absorption in each of three layers A_1 , A_2 , and A_3 as a function of tissue refractive index n_1 for $d_1 = 150 \mu\text{m}$, $d_2 = 50 \mu\text{m}$, $\mu_{a,1} = 0.05 \text{ mm}^{-1}$, $\mu_{a,2} = 1 \text{ mm}^{-1}$, $\mu_{a,3} = 0.01 \text{ mm}^{-1}$, $\mu'_{s,1} = 1 \text{ mm}^{-1}$, $\mu'_{s,2} = 0.5 \text{ mm}^{-1}$, $\mu'_{s,3} = 2 \text{ mm}^{-1}$, and n_1 is between 1 and 2, estimated by Monte Carlo simulations (symbols) and the three-layer analytic model (solid line). The relative percent error for each estimate is also shown.